Supporting information: Versatile shape recoverability of odd-numbered saturated long-chain fatty acid crystals

Satoshi Takamizawa* and Yuichi Takasaki

Abstract: Superelasticity, which has been known dominantly in association with a specific kind of alloy called shape-memory alloys, involves a peculiar recoverability after plastic deformation. However, metal superelasticity remains difficult in material applications requiring flexible and biocompatible usage. Herein we revealed the versatile recoverability including elasticity, superelasticity, ferroelasticity, and shape-memory effects of soft fatty acid crystals, which can be regarded as biological metabolites, providing new insights on organic materials for incredible shape recoverability.

Contents: **Page**

Main text figures **2-7**
(a) Experimental **8**
(b) Transition temperatures of straight-chain saturated fatty acids **9**
(c) X-ray diffraction **10-13**
(d) Uniaxial compression test of C15 crystals **14**
(e) Details in crystal deformations of C15 **14-15**
(f) DSC measurements **16**
(g) Superelastic transformations between A'$_h$ and A'$_l$ **17**
(h) Stress-strain test and its temperature dependency **18-20**
(i) Movies **21**
Supporting references **22**

Other materials:

Movie S1a-d, Movie S2a-c, Movie S3, Movie S4a-b, Movie S5, Movie S6a-b, Movie S7

Main text figures

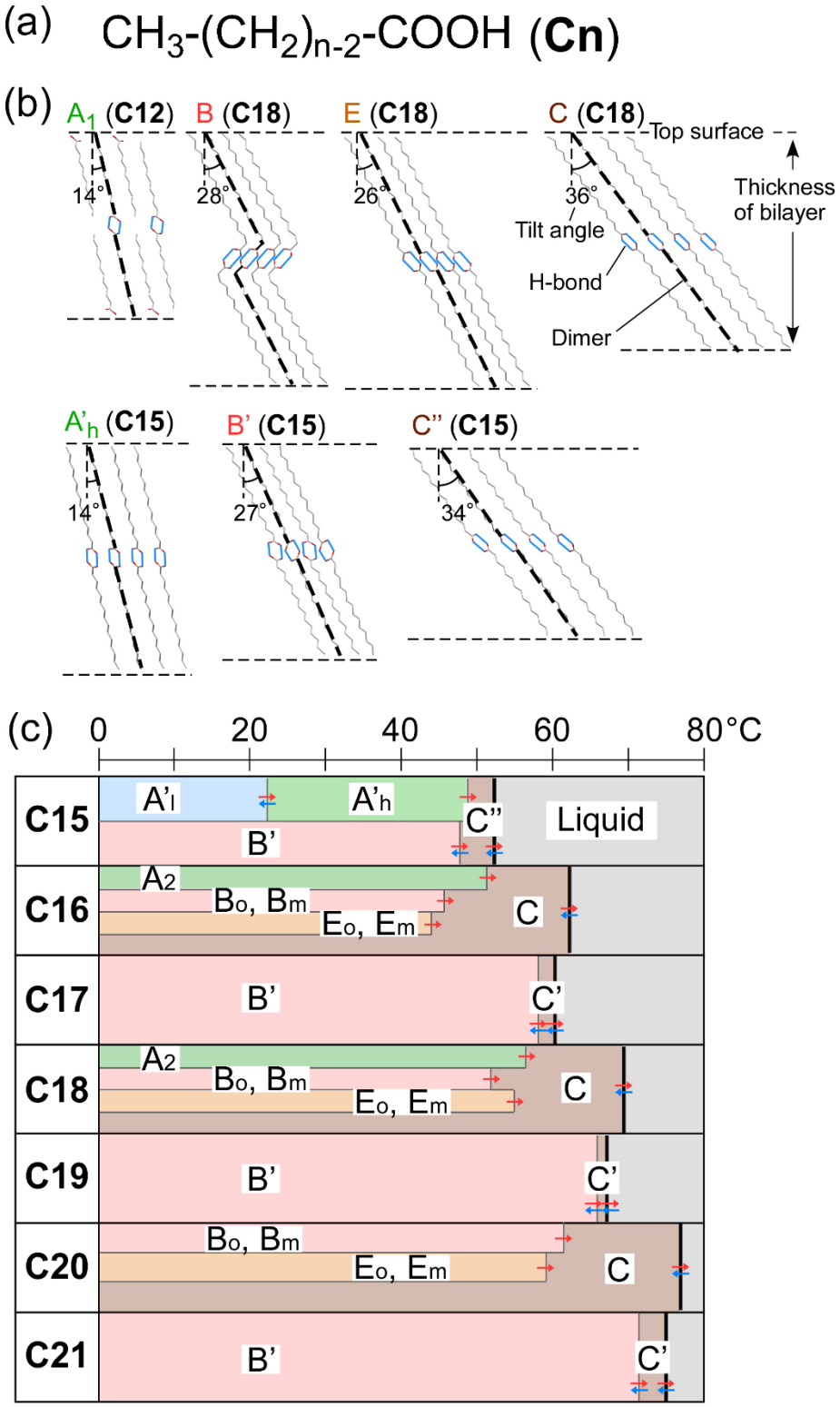

Figure 1

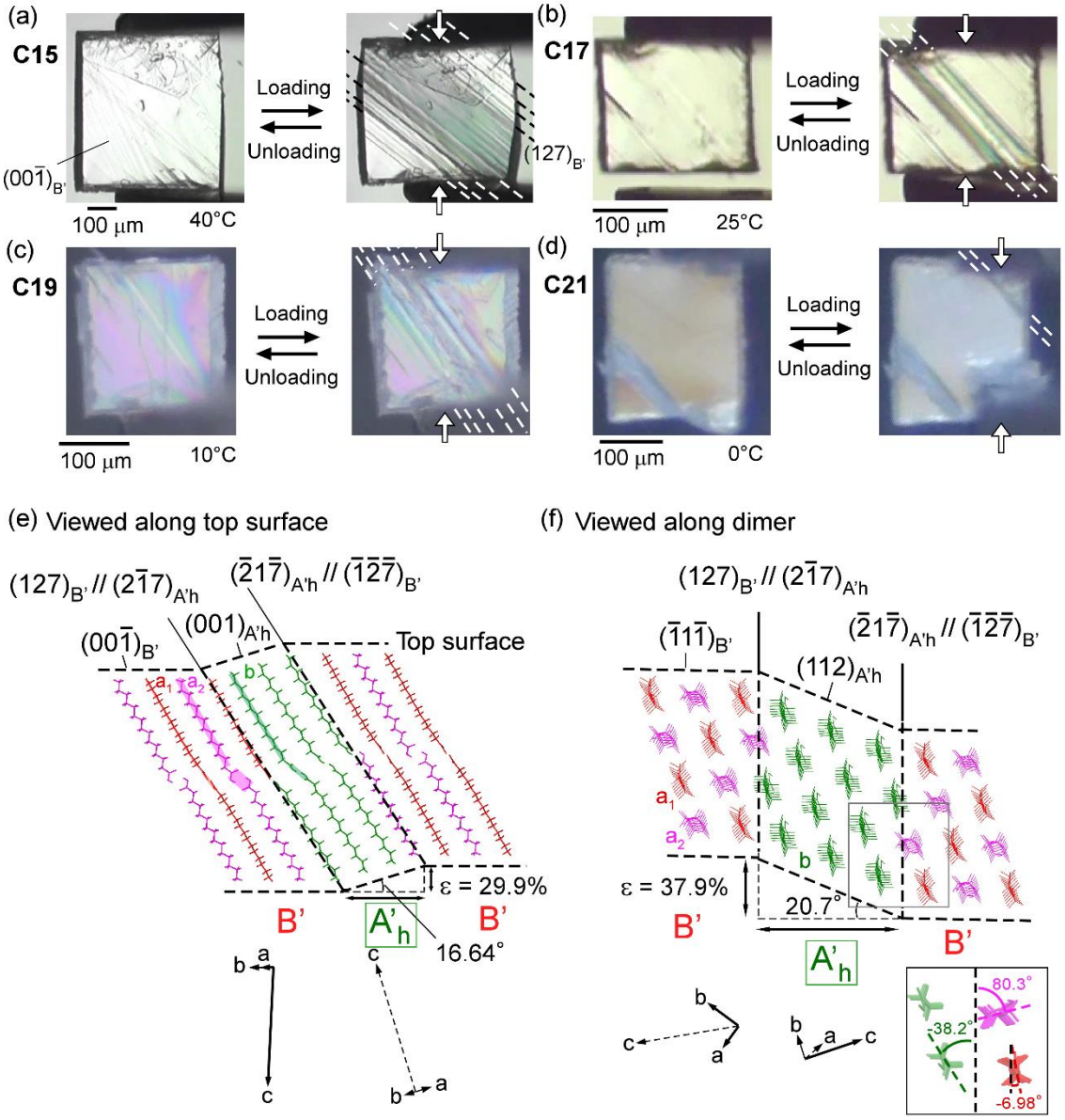
(a)
C15
Loading
Unloading
100 μm
40°C
(b)
C17
Loading
Unloading
100 μm
25°C
(c)
C19
Loading
Unloading
100 μm
10°C
(d)
C21
Loading
Unloading
100 μm
0°C
(e) Viewed along top surface
Top surface
ε = 29.9%
16.64°
B'
A'h
B'
(f) Viewed along dimer
ε = 37.9%
20.7°
B'
A'h
B'
80.3°
38.2°
-6.98°

Figure 2

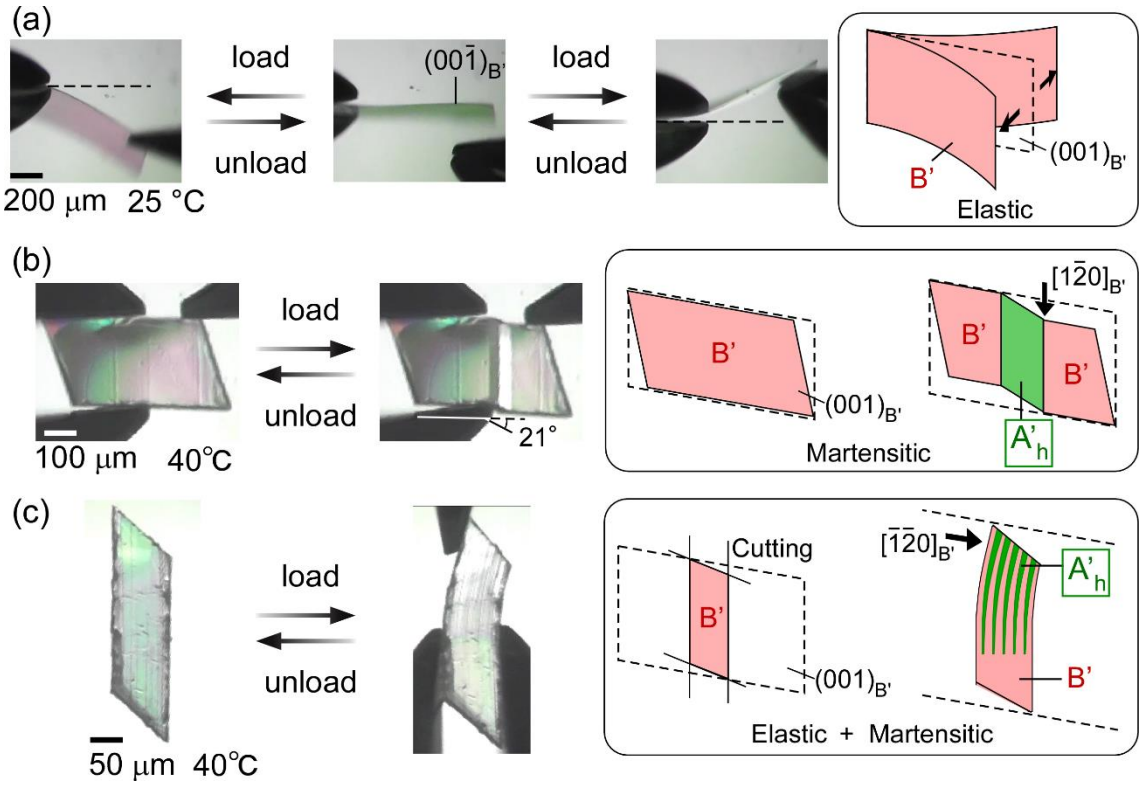
(a)
load
unload
load
unload
$(00\bar{1})_{B'}$
200 μm 25 °C
B'
$(001)_{B'}$
Elastic
(b)
load
unload
21°
100 μm 40°C
B'
$(001)_{B'}$
Martensitic
$[1\bar{2}0]_{B'}$
B'
B'
A'_h
(c)
load
unload
50 μm 40°C
Cutting
B'
$(001)_{B'}$
$[1\bar{2}0]_{B'}$
A'_h
B'
Elastic + Martensitic

Figure 3

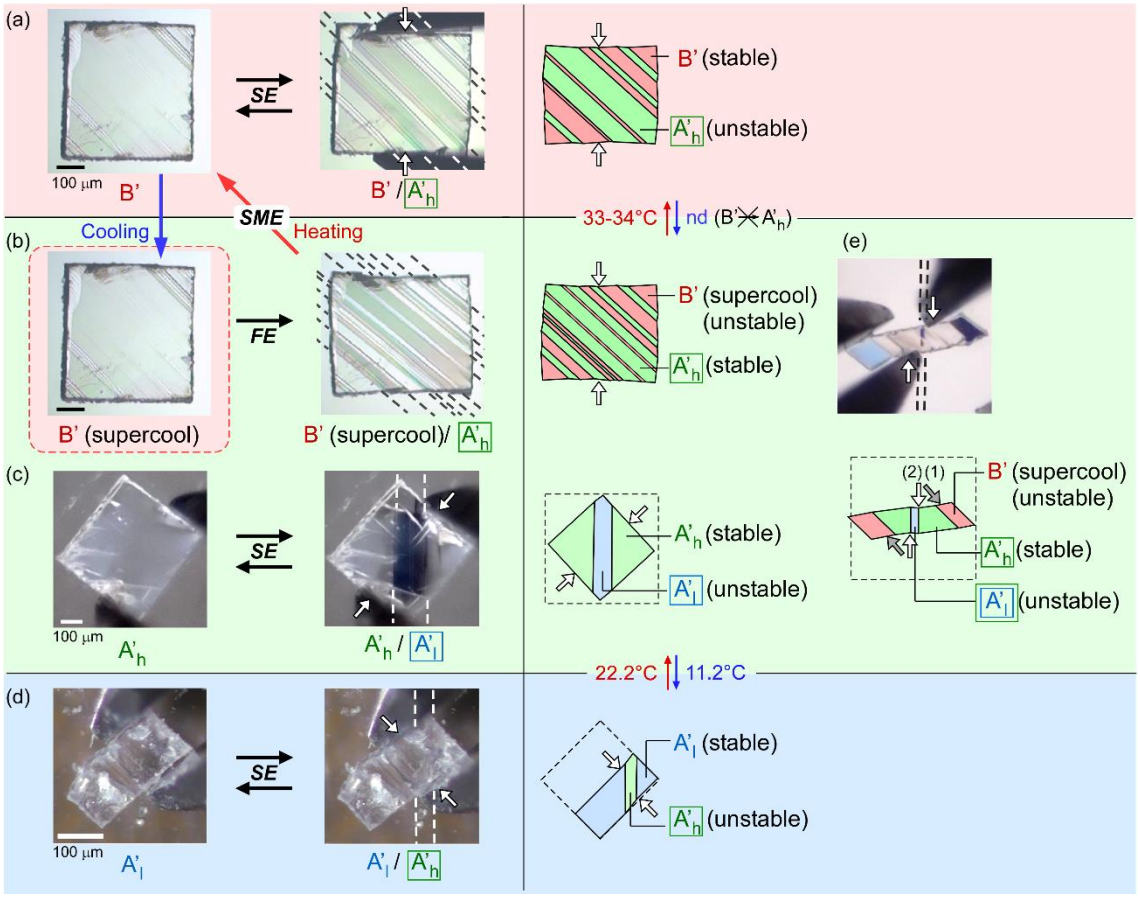
(a)
100 μm
B'
SE
B' / A'h
B' (stable)
A'h (unstable)
SME
Cooling
Heating
33-34°C
nd (B' ✕ A'h)
(b)
B' (supercool)
FE
B' (supercool)/ A'h
B' (supercool) (unstable)
A'h (stable)
(e)
(c)
100 μm
A'h
SE
A'h / A'l
A'h (stable)
A'l (unstable)
(2) (1)
B' (supercool) (unstable)
A'h (stable)
A'l (unstable)
22.2°C
11.2°C
(d)
100 μm
A'l
SE
A'l / A'h
A'l (stable)
A'h (unstable)

Figure 4

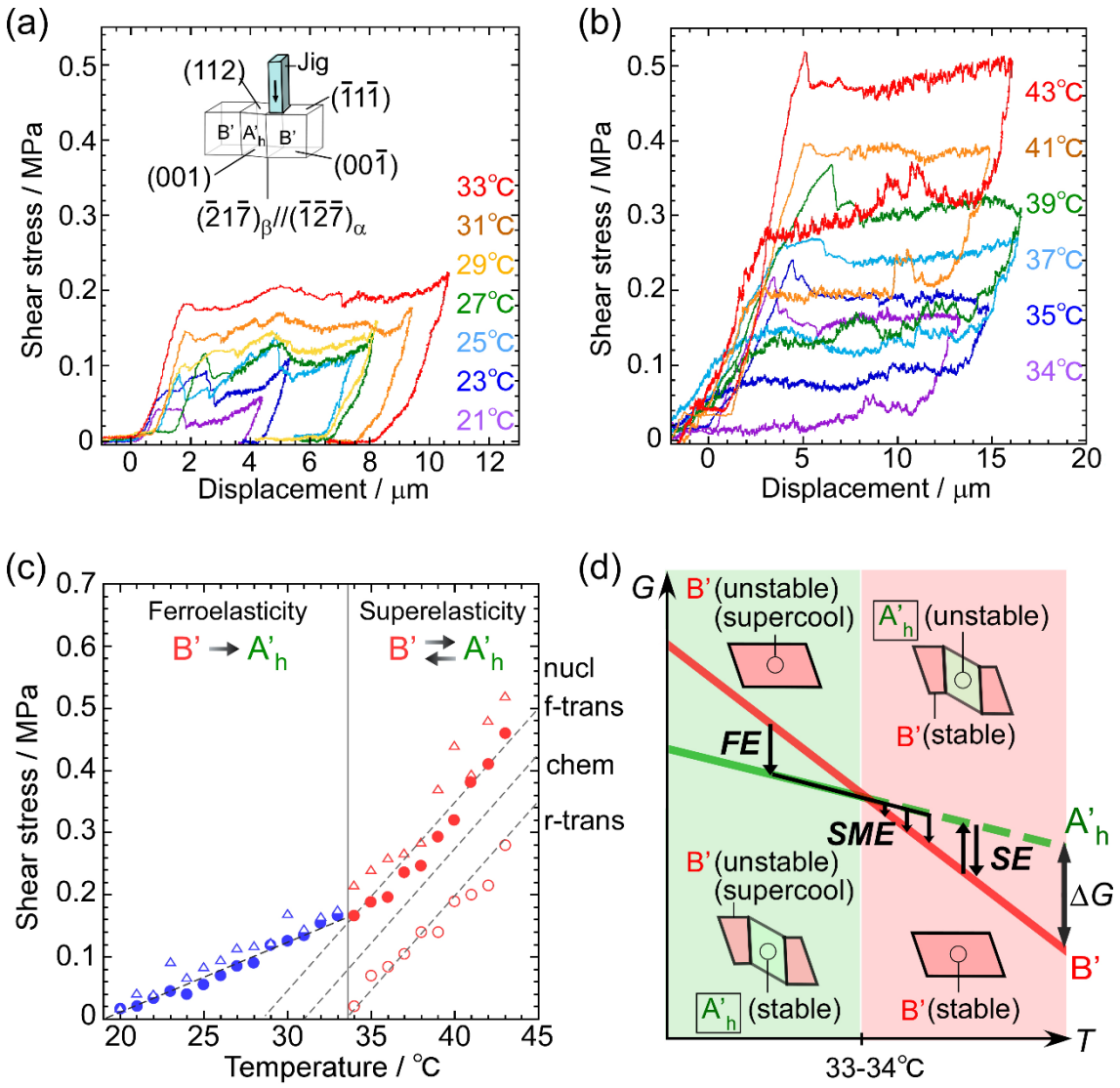
(a)
Shear stress / MPa
Displacement / μm
(112)
Jig
(1̄11̄)
B' A'h B'
(001)
(001̄)
(2̄17̄)β//(1̄27̄)α
33℃
31℃
29℃
27℃
25℃
23℃
21℃
(b)
Shear stress / MPa
Displacement / μm
43℃
41℃
39℃
37℃
35℃
34℃
(c)
Shear stress / MPa
Temperature / ℃
Ferroelasticity
B' → A'h
Superelasticity
B' ⇄ A'h
nucl
f-trans
chem
r-trans
(d)
G
T
B' (unstable) (supercool)
A'h (unstable)
B' (stable)
FE
SME
SE
ΔG
A'h
B'
B' (unstable) (supercool)
A'h (stable)
B' (stable)
33-34℃

Figure 5

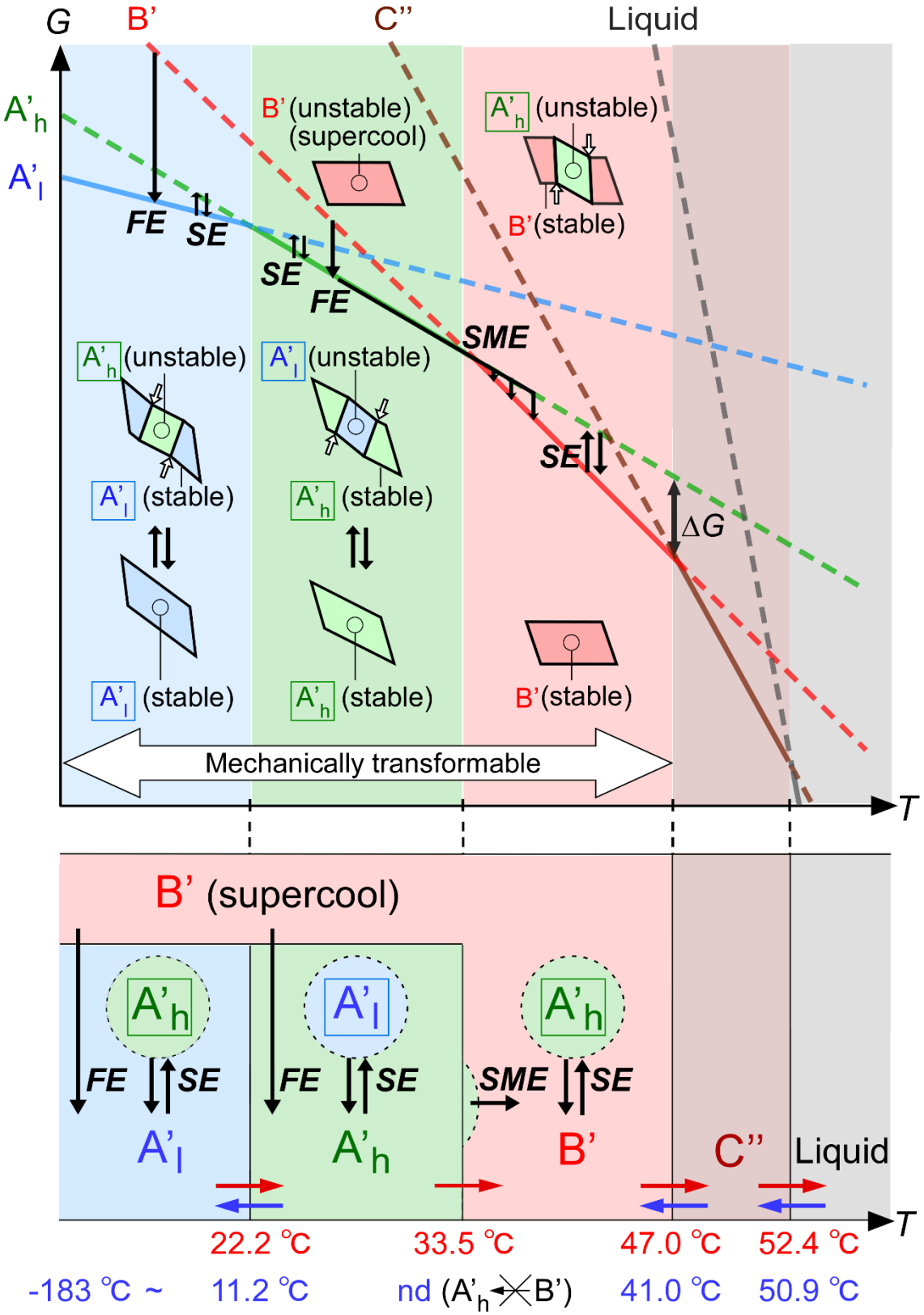
G
B'
C''
Liquid
A'h
A'l
B'(unstable)
(supercool)
A'h (unstable)
B'(stable)
FE
SE
SE
FE
SME
A'h (unstable)
A'l (unstable)
SE
A'l (stable)
A'h (stable)
ΔG
A'l (stable)
A'h (stable)
B'(stable)
Mechanically transformable
T
B' (supercool)
A'h
A'l
A'h
FE
SE
FE
SE
SME
SE
A'l
A'h
B'
C''
Liquid
T
22.2 ℃
33.5 ℃
47.0 ℃
52.4 ℃
-183 ℃ ~
11.2 ℃
nd (A'h ✕ B')
41.0 ℃
50.9 ℃

Figure 6

(a) Experimental

i) Preparation of crystals. The crystals of fatty acids were purchased from Tokyo Chemical Industry and were used as received. Single crystals were prepared by recrystallization from a concentrated solution in isooctane.

ii) Single-crystal X-ray diffraction experiment

Single-crystal X-ray analysis was performed around room temperature on a Bruker SMART APEX CCD area (graphite-monochromated Mo-Kα radiation (λ = 0.71073 Å) with a nitrogen flow temperature controller. Empirical absorption corrections were applied using the SADABS program. The structure was solved by direct methods (SHELXS-97) and refined by full-matrix least squares calculations on F^2 (SHELXL-97) using the SHELX-TL program package. Non-hydrogen atoms were refined anisotropically; hydrogen atoms were refined in a riding model. The crystal face indexing was carried out using SMART in a SHELXTL Ver.6.12 program package with a twin resolution program. Crystallographic data of the structure is summarized in Tabs. S1 and S2. The shear-stressed form during superelastic deformation was fixed with resin.

iii) Microscope observations

A polarized light microscope microscope coupled with a digital camera was used to record mechanical deformation.

iv) Stress-strain test

Shear tests were carried out on a universal testing machine (Tensilon RTG-1210, A&D Co. Ltd.).

v) DSC measurements

DSC measurements were carried on a thermal analysis equipment (DSC-60, Shimadzu Co. Ltd.)

(b) Transition temperatures of straight-chain saturated fatty acids

Table S1. Transition temperatures of reported polymorphs of **C12-C21**.

Compound	Phase change	T_{trans} (°C)	T_{mp} (°C)	Ref [b]
$C_{12}H_{24}O_2$ (Lauric acid, **C12**)	$A_{super} \rightarrow C$	34.95	45.0	[S1]
$C_{13}H_{26}O_2$ (Tridecanoic acid, **C13**)	$A'_l \rightarrow A'_h$	14.55	41.85	This work
	$A'_h \rightarrow C''$	35.95		This work
$C_{14}H_{28}O_2$ (Myristic acid, **C14**)	$A_2 \rightarrow C$	41.85	55.89	[S1]
	$A_{super} \rightarrow C$	52.15		[S1]
$C_{15}H_{30}O_2$ (Pentadecanoic acid, **C15**)	$A'_l \rightarrow A'_h$	22.35	52.35	[S2]
	$A'_h \rightarrow B'$	33.5		This work
	$A'_h \rightarrow C''$	47.65		[S2]
	$B' \rightarrow C''$	46.45		This work
$C_{16}H_{32}O_2$ (Palmitic acid, **C16**)	$A_2 \rightarrow C$	51.55	63.44	[S1]
	$A_{super} \rightarrow C$	57.85		[S1]
	$E_m \rightarrow C$	43.55		[S1]
	$B_m \rightarrow C$	44.35		[S1]
$C_{17}H_{34}O_2$ (Heptadecanoic acid, **C17**)	$B' \rightarrow C'$	57.40	60.10	This work
$C_{18}H_{36}O_2$ (Stearic acid, **C18**)	$A_2 \rightarrow C$	58.45	69.45	[S1]
	$E_m \rightarrow C$	54.55		[S1]
	$B_m \rightarrow C$	51.25		[S1]
	$B_o \rightarrow C$	52.75		[S1]
$C_{19}H_{38}O_2$ (Nonadecanoic acid, **C19**)	$B' \rightarrow C'$	65.76	66.16	This work
$C_{20}H_{40}O_2$ (Arachidic acid, **C20**)	$E_m \rightarrow C$	59.65	77.01	[S1]
	$B_m \rightarrow C$	59.45		[S1]
	$B_o \rightarrow C$	60.15		[S1]
$C_{21}H_{42}O_2$ (Heneicosanoic acid, **C21**)	$B' \rightarrow C'$	71.29	75.76	This work

(c) X-ray diffraction

Table S2. Crystallographic data of **C15**.

Crystal phase	A'_l	A'_h	B'
Morphology*	Bent (A'_l/A'_h)	Bent (A'_h/B')	Bent (A'_h/B')
Empirical formula	$C_{15}H_{30}O_2$	$C_{15}H_{30}O_2$	$C_{15}H_{30}O_2$
Crystal size /mm^3	0.70×0.50×0.15	1.19×1.10×0.18	1.19×1.10×0.18
M	242.39	242.39	242.39
Crystal system	Triclinic	Triclinic	Triclinic
Space group	$P\bar{1}$	$P\bar{1}$	$P\bar{1}$
T /K	289	303	303
a /Å	4.905(3)	4.286(4)	5.554(2)
b /Å	8.103(4)	4.944(4)	8.083(3)
c /Å	39.77(2)	40.10(4)	35.965(15)
α /deg	90.409(12)	87.272(18)	88.037(9)
β /deg	92.129(10)	88.197(16)	87.514(8)
γ /deg	102.813(12)	68.316(18)	79.973(9)
V /Å^3	1540.1(14)	788.5(12)	1587.7(11)
Z	4	2	4
D_{calcd} / Mg m^{-3}	1.045	1.021	1.014
μ(Mo Kα) / mm^{-1}	0.067	0.065	0.065
Reflections collected	7304	5461	11614
Independent reflections (R_{int})	1634 (0.0635)	869 (0.0780)	2840 (0.0367)
Goodness of fit	1.285	0.990	0.935
R_1(I > 2σ (all data))	0.1960 (0.3410)	0.1487 (0.3466)	0.0825 (0.2118)
wR_2(I > 2σ (all data))	0.5023 (0.5592)	0.3980 (0.4867)	0.2131 (0.2987)
Largest diff. peak (hole) /eÅ^3	0.529 (-0.654)	0.540 (-0.407)	0.363 (-0.325)
CCDC registry number	CCDC 1846957	CCDC 1846958	CCDC 1846959

*Bent shapes were mechanically produced by applying shear force on the as-synthesized B' crystal.

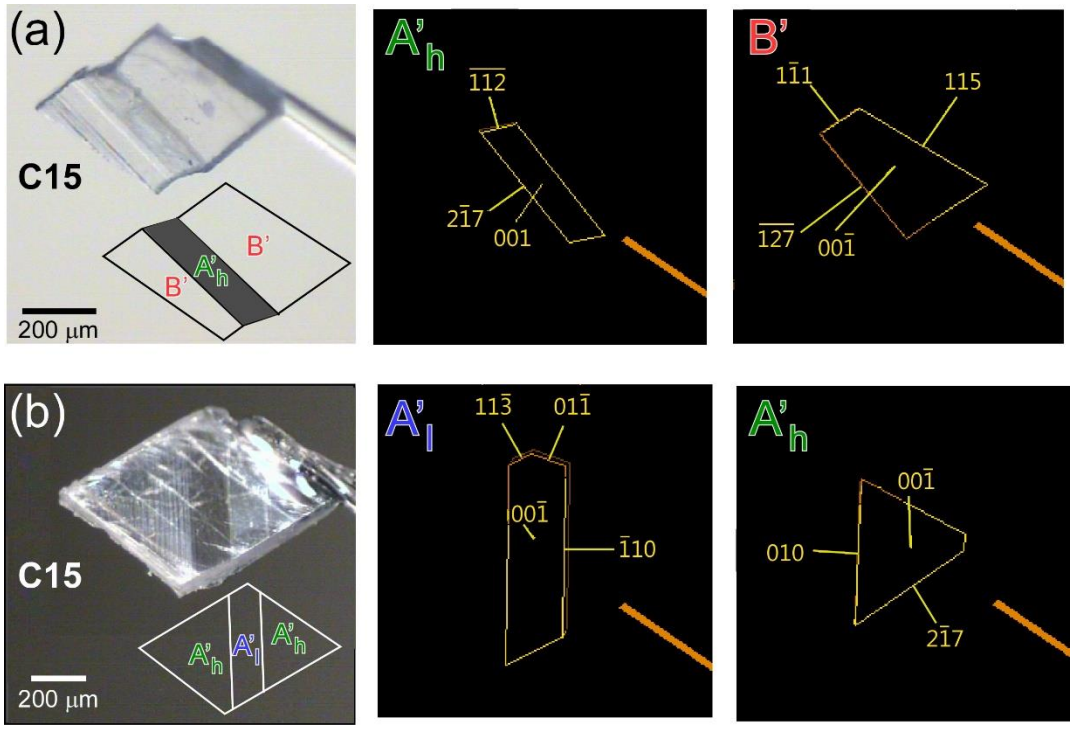

Figure S1. Crystal face indexing of **C15** under A'_h/B' coexisting states at 300 K (a) and A'_l/A'_h coexisting states at 289 K (b).

Table S3. Cell parameters of a mechanically bent crystal of **C17**.

Crystal phase	A'_h *	B'
Morphology*	Bent (A'_h/B')	Bent (A'_h/B')
Empirical formula	$C_{17}H_{34}O_2$	$C_{17}H_{34}O_2$
Crystal size /mm^3	0.61×0.36×0.06	0.61×0.36×0.06
M	242.39	242.39
Crystal system	Triclinic	Triclinic
Space group	-	$P\bar{1}$
T /K	298	298
a /Å	4.2790	5.57(2)
b /Å	4.8823	8.07(3)
c /Å	44.7828	40.52(15)
α /deg	91.4772	88.89(4)
β /deg	92.0642	88.80(4)
γ /deg	110.2728	80.20(4)
V /Å^3	876.323	1795(12)
Z	2	4
D_{calcd} / Mg m^{-3}	-	1.001
μ(Mo Kα) / mm^{-1}	-	0.063
Reflections collected	-	5931
Independent reflections (R_{int})	-	1448 (0.060)
Goodness of fit	-	0.973
R_1(I > 2σ (all data))	-	0.1495 (0.3210)
wR_2(I > 2σ (all data))	-	0.3800 (0.4878)
Largest diff. peak (hole) /eÅ^3	-	0.240 (-0.296)
Supporting CIF file		C17.cif

* Only the cell parameter has been confirmed as A'_h in terms of similarity to A'_h in **C15**.

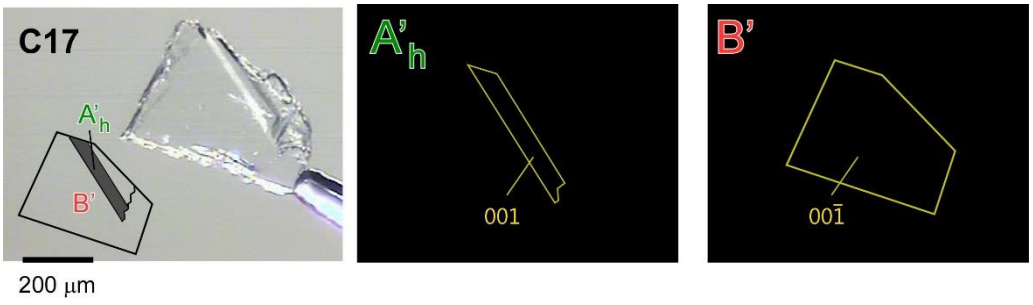

Figure S2. Crystal face indexing of **C17** under A'_h/B' coexisting states at 298 K.

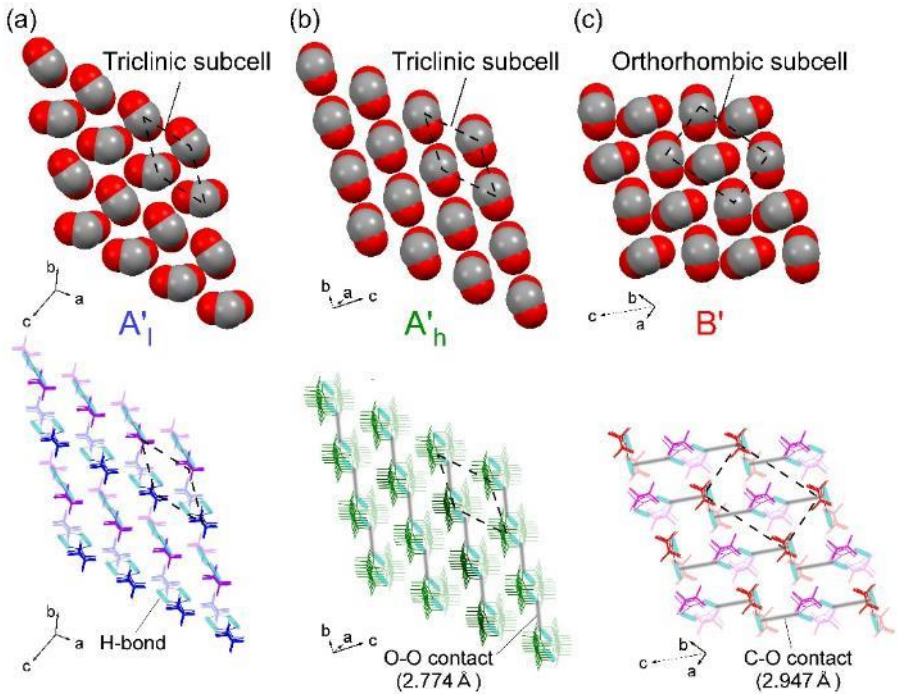

Figure S3. Orientations of neighboring carboxylic moieties in A'$_l$ (a), A'$_h$, (b) and B' phases (c) in **C15** viewed along the alkyl chain axes. (Upper: the face on the carboxylic groups in a space-filling model, lower: view of a stick model.)

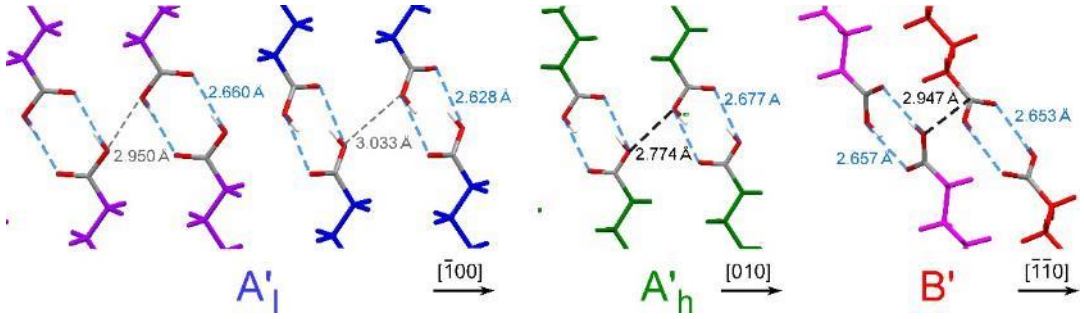

Figure S4. Hydrogen bonding moieties and interdimer contacts in various crystal phases of **C15** with perpendicular views. (Dotted lines indicate dimerization (Blue), short contact between O-O and O-C atoms (black), and the atomic distance between O-O atoms (gray).)

(d) Uniaxial compression test of **C15** crystals

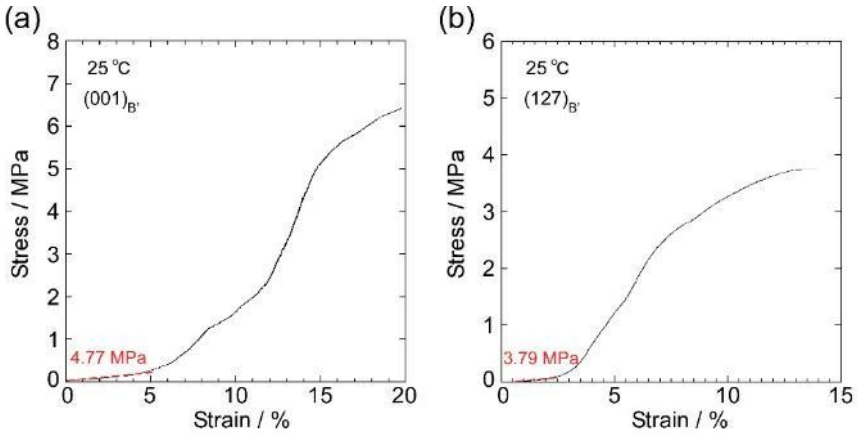

Figure S5. Stress-strain curves in uniaxial compressions of **C15** crystals at 25 °C. Compression along the normal direction of the top surface of the crystal $(001)_{B'}$ (a) and along the normal direction of the A'_h/B' phase interface $(127)_{B'}$ (b). The Young's moduli were estimated from each initial slope of the additional red dotted lines. (The largest Young's moduli can be estimated just before the yielding point as 93.5 MPa with a strain of 12-15% for (a) and 58.6 MPa with a strain of 4-7% for (b).

(e) Details in crystal deformations of **C15**

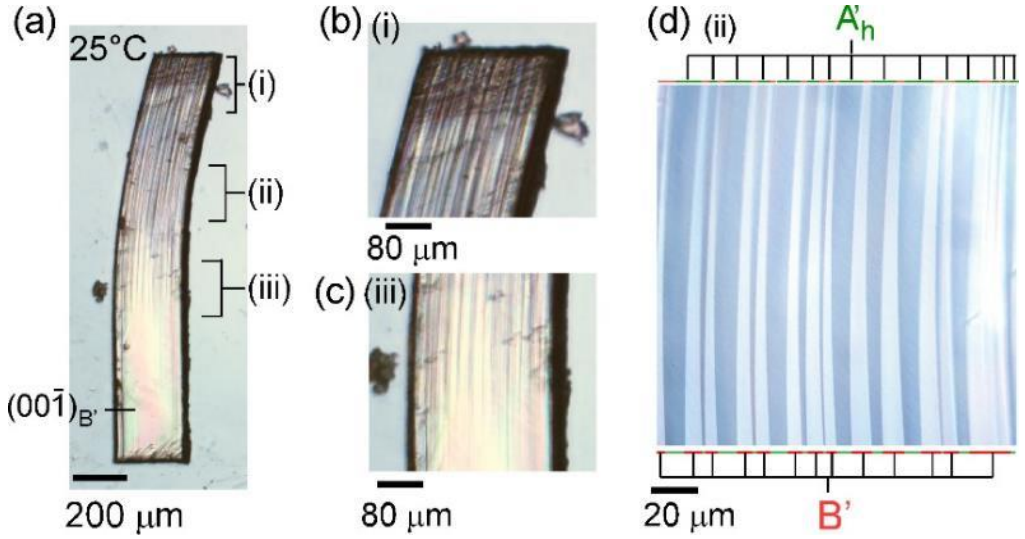

Figure S6. Magnified photographs of **C15** sheared by loading perpendicular to $[1\text{-}20]_{B'}$ (a): the enlarged images of the parts at i-iii (b-d).

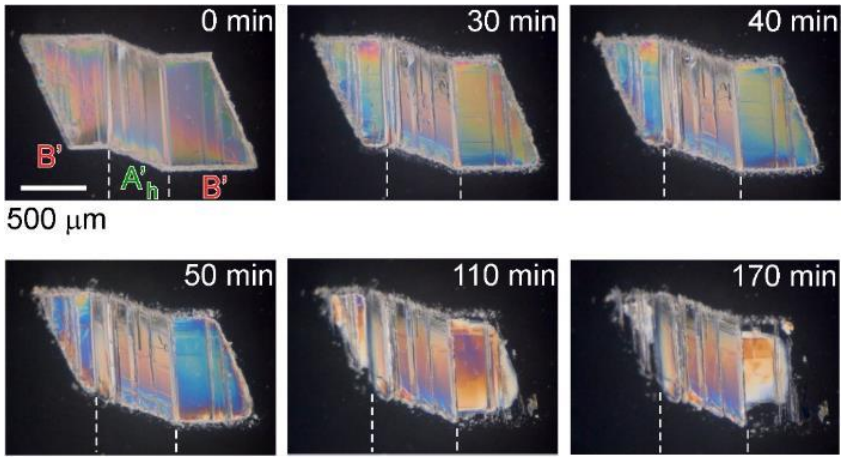

Figure S7. Spontaneous phase transition of ferroelastic **C15** from shear-induced A'$_h$ to mother B' in a saturated isooctane solution at 24 °C, which agrees with the crystal being thermally unstable at 24 °C. The lower stability of supercooled B' is also indicated by the higher solubility in the solution than that of the thermally stable A'$_h$.

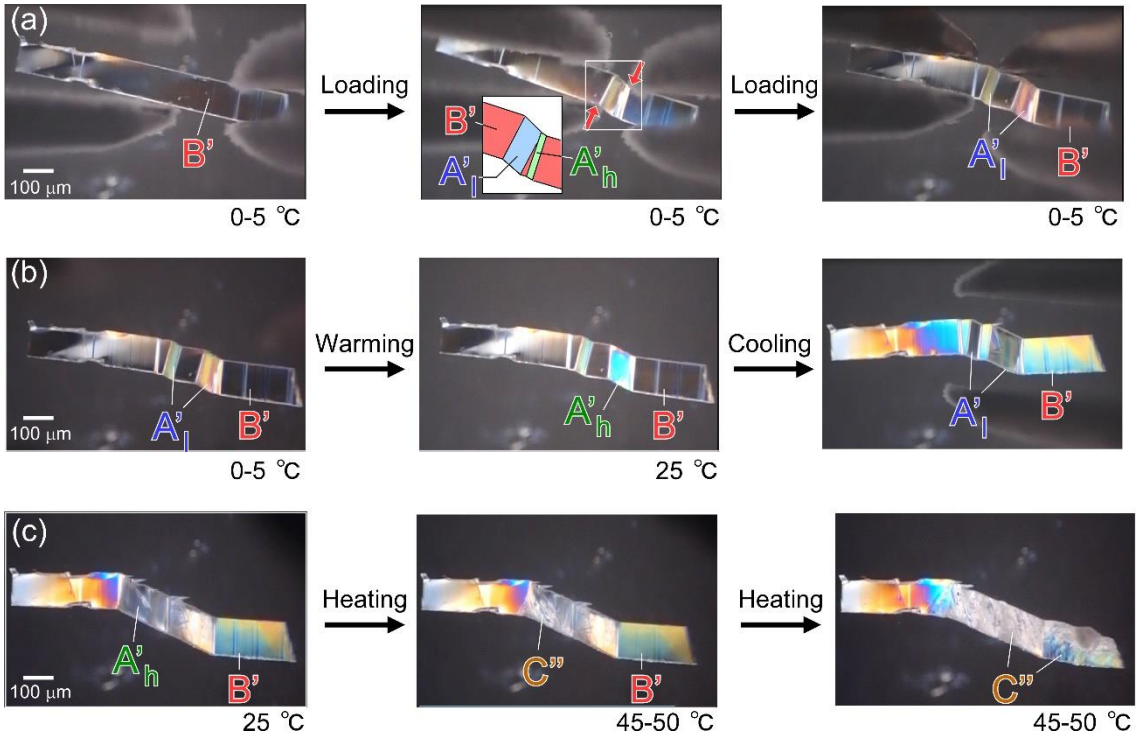

Figure S8. Cogeneration and phase transitions among various phases in the crystal of **C15** at various temperatures: generation of the A'$_l$ domain from supercooled B' crystal by slight mechanical stimulation (a), thermal interchangeability between A'$_l$ and A'$_h$ (b), and thermal-induced transformation into C'' from both A'$_h$ and B' with a slight time lag by applying heat to the crystal (c). (See Movie S5.) The thermal correlation between crystal phases is coincident with the results of DSC measurements displayed in Fig. S9.

(f) DSC measurements

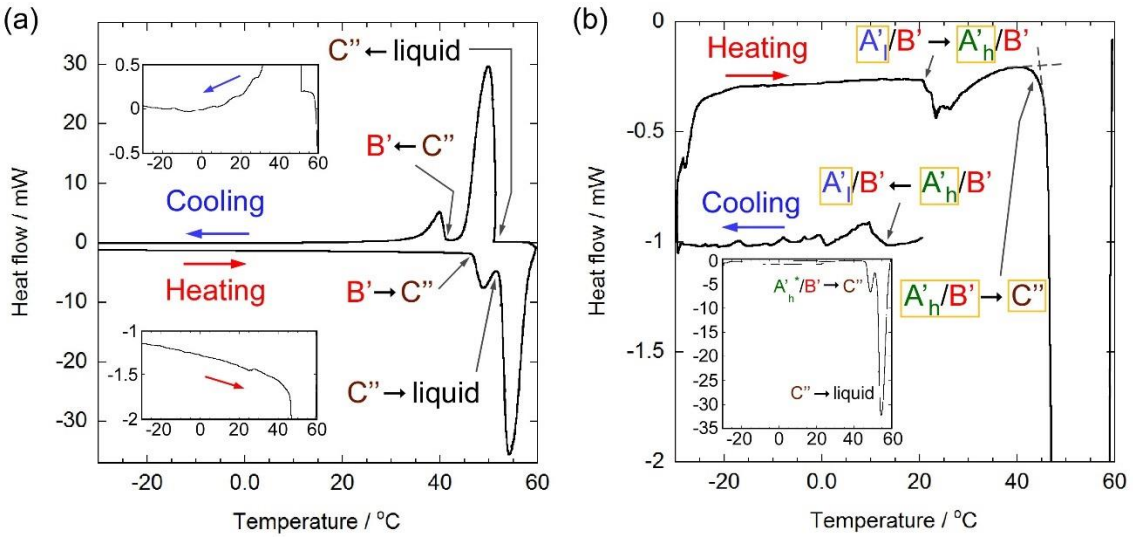

Figure S9. DSC data for **C15**: as-synthesized B' crystals (a) and stress-induced A'$_h$/B' coexisting crystals (b). (The phase change from B' into C'' occurred at 48.04 °C by heating, and the crystal melted at 53.24 °C. (a) Solidification to C'' occurred at 49.96 °C, and it changed into B' at 41.49 °C upon cooling. The B' remained in a supercool sate even at -30 °C. For the stress-induced A'$_h$/B' coexisting crystal (volume fraction of 25:75), A'$_h$ transitioned to A'$_l$ at 11.16 °C with initial cooling (b). The A'$_l$ phase reversibly changed to A'$_h$ at 22.23 °C with subsequent heating, and both A'$_h$ and B' phases changed to the C'' phase at 46.54 °C.)

Table S4. Transition temperatures (T_{trans}) and enthalpies (ΔH) of **C15** estimated by DSC data. Phase transitions from A'$_h$ were investigated using deformed B' crystals that included A'$_h$ domains (fraction of 25 - 50%).

		This work (single crystals)		References (powder)	
		$T_{0\pm\delta}$ (°C)	ΔH (kJ mol^{-1})	$T_{0\pm\delta}$ (°C)	ΔH (kJ mol^{-1})
(1) A'$_l$ / B' ⇄ A'$_h$ / B'	Heating (→)	22.23	0.37	22.4 [S1]	0.27 [S1]
	Cooling (←)	11.16	0.45	20.7 [S2]	1.4 [S2]
(2) B' ⇄ C''	Heating (→)	46.96	4.27	45.6 [S1]	8.2 [S1]
	Cooling (←)	41.04	3.54	–	–
(3) C'' ⇄ liquid	Heating (→)	52.40	38.3	52.4 [S1]	40.4 [S1]
	Cooling (←)	50.91	42.5	–	–

(g) Bipolar superelastic transformations between A'$_h$ and A'$_l$

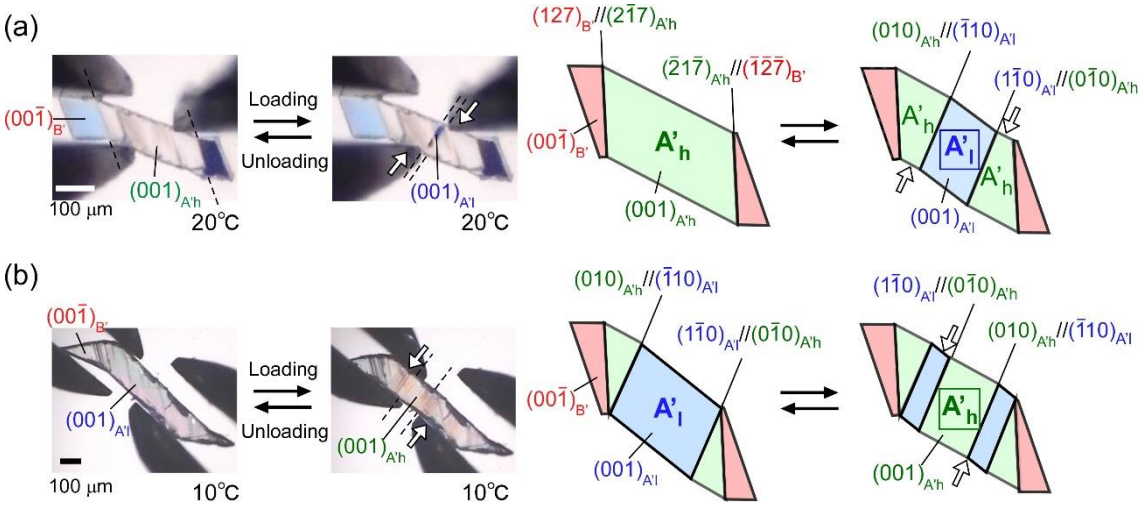

Figure S10. Interchange of the direction of phase transition for bipolar superelastic transformations from A'$_h$ to unstable A'$_l$ at 20°C (a) and from A'$_l$ to unstable A'$_h$ at 10°C (b). These were recorded under a polarized microscope. (Movie S6a,b)

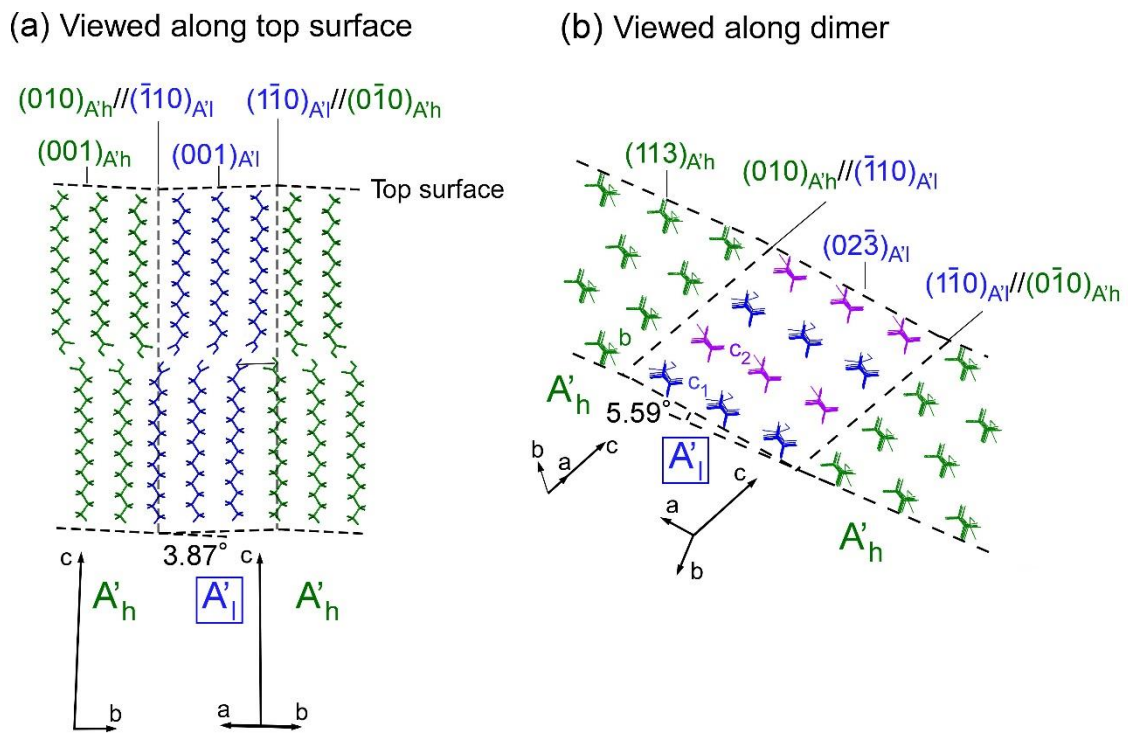

Figure S11. Packing diagram of A'$_h$ and A'$_l$ in the coexistent state, as determined by single-crystal X-ray structure analysis for the mechanically bent crystal at 289 K: crystal structures viewed along the top surface of the A'$_h$ crystal ((001)$_{A'h}$) (a) and along each dimer (b). The inter-plane angle between the A'$_l$/A'$_h$ interface and the A'$_h$/B' interface is 50.3°.

(h) Stress-strain test and its temperature dependency

Table S5. Summary of the conditions for the stress-strain tests on **C15** crystals.

Temperature / °C	Loading surface	Crystal dimension		Press type		Displacement velocity/ μm min^{-1}	Correspondence
		Width/ μm	Thickness / μm	Contact area/ m^2	Jig (width / μm)		
21-33	$(\bar{1}\bar{1}1)$	156	167	1.48×10^{-8}	Blade (95)	50	Fig. 5a, S11b
34-43	$(\bar{1}\bar{1}1)$	63	414	9.14×10^{-9}	Blade (145)	50	Fig. 5b, S11c

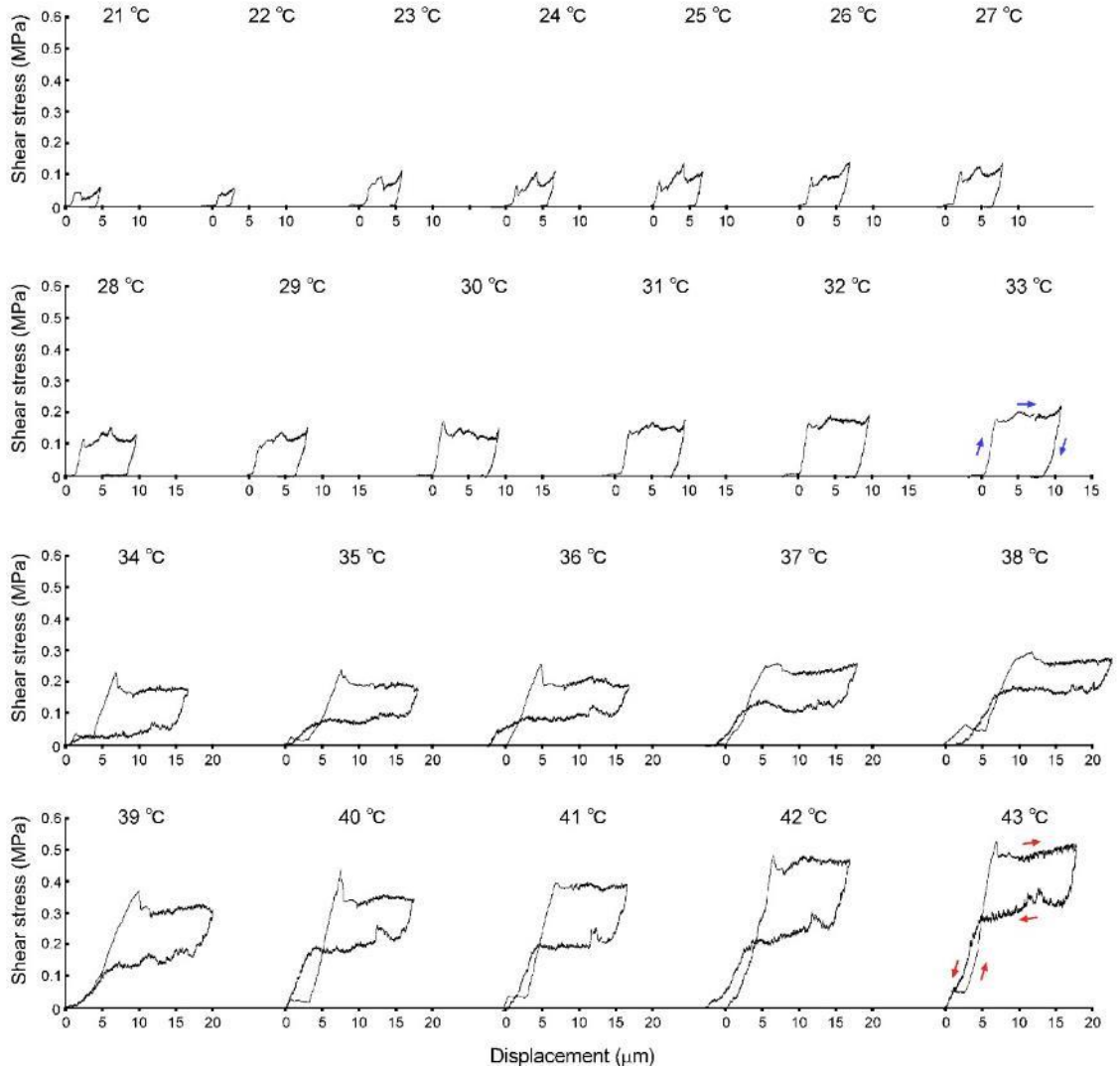

Figure S12. Stress-strain curves at various temperatures obtained using the crystal specimens listed in Table S5. (21-33 °C: martensitic ferroelastic transformations; 34-43 °C: martensitic superelastic transformations.)

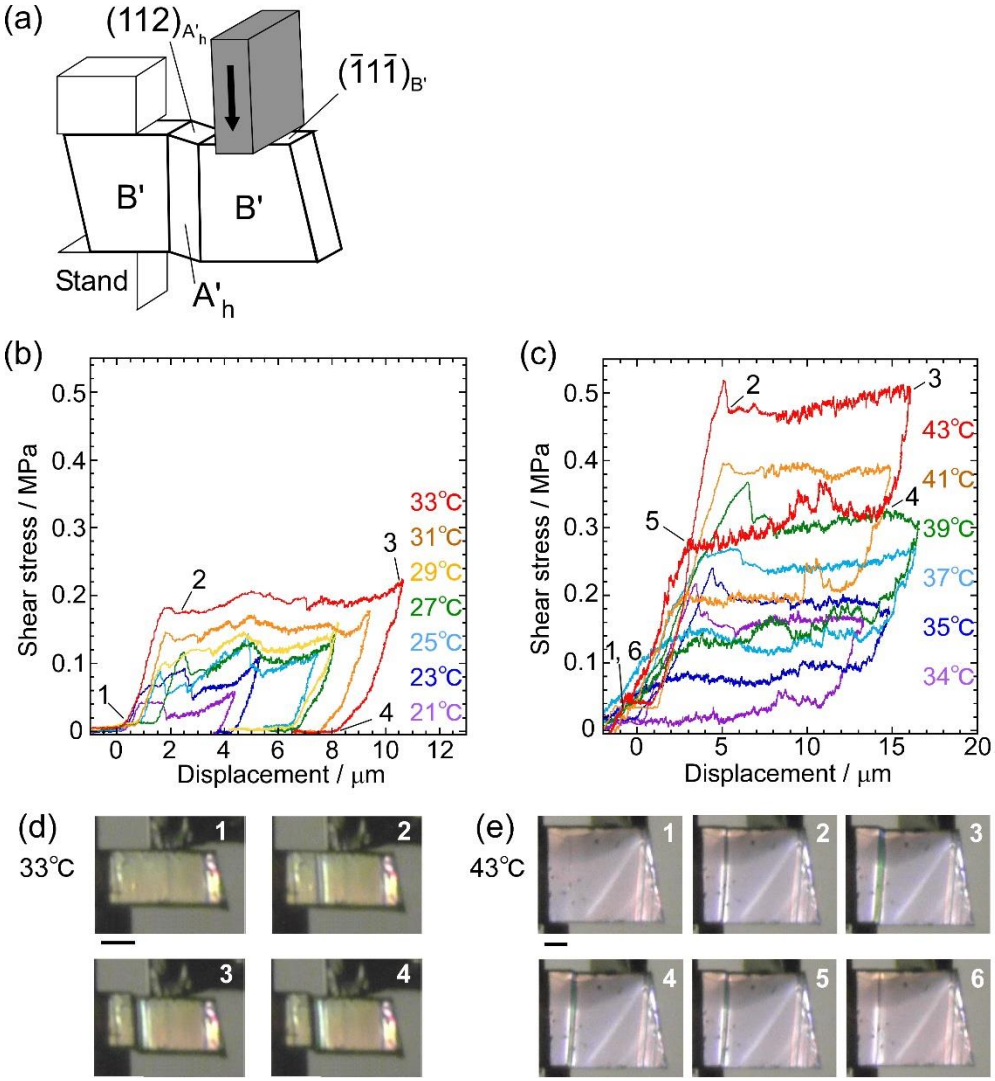

Figure S13. The mechanical coordinates for the stress-strain tests of **C15** (a). Stress-strain curves in the ferroelastic region (b) and superelastic region (c). Snapshots taken during the tests at 33 °C (d) and 43 °C (f) under a polarizing microscope. Scale bars indicate 100 μm.

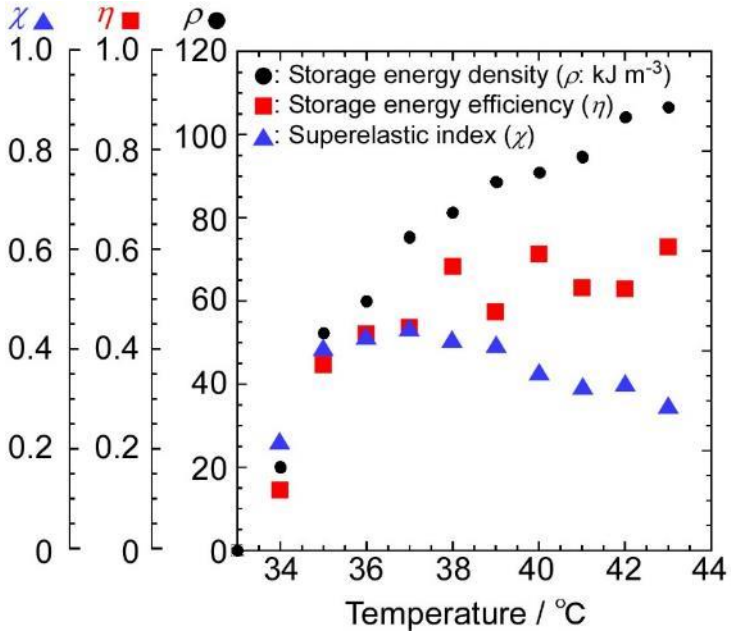

Figure S14. Temperature dependence of the energy storage density (black), energy storage efficiency (red), and superelastic index (blue) in the superelastic region. The values are summarized in Table S6.

Table S6. Principal indexes of the superelastic parameters of the **C15** crystal at various temperatures plotted in Fig. S12.*

Temperature (°C)	Energy density (ρ) (kJ m^{-3}) [(J g^{-1})]	Energy efficiency (η)	Superelastic index (χ)
34	20.2 [0.198]	0.121	0.218
35	52. 4 [0.0515]	0.372	0.406
36	60.1 [0.059]	0.434	0.428
37	75.5 [0.0742]	0.447	0.444
38	81.3 [0.0800]	0.569	0.421
39	88. 8 [0.0873]	0.478	0.410
40	91.0 [0.0894]	0.594	0.357
41	94.8 [0.0933]	0.526	0.327
42	104 [0.102]	0.524	0.333
43	107 [0.105]	0.609	0.288

*The parameters were calculated with the density fixed at 1.017 Mg m^{-3}, which was given by X-ray data for the B' phase of **1** at 303 K. ($\rho=W_{r\text{-}trans}/V_{f\text{-}trans}$; $\eta=W_{r\text{-}trans}/W_{f\text{-}trans}$; $\chi=\rho/\sigma_{chem}$: W means work input (f-trans) or output (r-trans) during transformation.)

Movies

Movie S1a: Superelastic transformation of compressed **C15** between B’ and stress-induced A'h at 40°C.
Movie S1b: Superelastic transformation of compressed **C17** between B’ and stress-induced A'h at 25°C.
Movie S1a: Superelastic transformation of compressed **C19** between B’ and stress-induced A'h at 10°C.
Movie S1b: Superelastic transformation of compressed **C21** between B’ and stress-induced A'h at 0°C.

Movie S2a: Elastic deformation of **C15** under supercooling B’at 25°C.
Movie S2b: Superelastic bending of **C15** between B’ and stress-induced A'h at 40°C.
Movie S2c: Thermal shape restoration of curved **C15** though the thermal transition from A'h to B' by the elevating temperature from 25°C to 40°C.

Movie S3: Shape-memory effect of compressed **C15** though the thermal transition from A'h to B' by the elevating temperature from 25°C to 40°C.

Movie S4a: Superelastic transformation of **C15** from A'h to stress-induced A'l at 20°C.
Movie S4b: Superelastic transformation of **C15** from A'l to stress-induced A'h at 10°C.

Movie S5: Various phases generation of **C15** at various temperatures. (See the caption of Figure S8.)

Movie S6a: Superelastic transformation of **C15** from A'h to stress-induced A'l within B’ crystal at 20°C.
Movie S6b: Superelastic transformation of **C15** from A'l to stress-induced A'h within B’ crystal at 10°C.

Movie S7: The video recorded during the measurements of stress-strain curves for the **C15** crystal: ferroelastic bending from supercooling B’ to A'h at 33°C (left) and superelastic deformation between B’ and stress-induced A'h (right) at 43°C. (Figure 5a-b, FigureS13)

Supporting references

[S1] E. Moreno, R. Cordobilla, T. Calvet, M. A. Cuevas-Diarte, G. Gbabode, P. Negrier, D. Mondieig, H. A. J. Oonk, *New J. Chem.*, **2007**, *31*, 947-957.

[S2] G. Gbabode, P. Negrier, D. Mondieig, E. M. Calvo, T. Calvet, M. A. Cuevas-Diarte, *Chem. Eur. J.* **2007**, *13*, 3150 – 3159.